ACS Photonics

Article

pubs.acs.org/journal/apchd5

Open Access on 07/18/2015

Nonlinear Midinfrared Photothermal Spectroscopy Using Zharov Splitting and Quantum Cascade Lasers

Alket Mertiri,[†,‡] Hatice Altug,[‡,§,∥] Mi K. Hong,[‡,⊥] Pankaj Mehta,[⊥] Jerome Mertz,[‡,#] Lawrence D. Ziegler,[‡,○] and Shyamsunder Erramilli*[,‡,⊥,#]

[†]Division of Materials Science and Engineering, [‡]Photonics Center, [§]Department of Electrical and Computer Engineering, [⊥]Department of Physics, [#]Department of Biomedical Engineering, and [○]Department of Chemistry, Boston University, Boston, Massachusetts 02215, United States

[∥]Department of BioEngineering, Ecole Polytechnique Federale De Lausanne, Lausanne, CH-1015, Switzerland

Supporting Information

ABSTRACT: We report on the mid-infrared nonlinear photothermal spectrum of the neat liquid crystal 4-octyl-4′-cyanobiphenyl (8CB) using a tunable Quantum Cascade Laser (QCL). The nonequilibrium steady state characterized by the nonlinear photothermal infrared response undergoes a supercritical bifurcation. The bifurcation, observed in heterodyne two-color pump−probe detection, leads to ultrasharp nonlinear infrared spectra similar to those reported in the visible region. A systematic study of the peak splitting as a function of absorbed infrared power shows the bifurcation has a critical exponent of 0.5. The observation of an apparently universal critical exponent in a nonequilibrium state is explained using an analytical model analogous of mean field theory. Apart from the intrinsic interest for nonequilibrium studies, nonlinear photothermal methods lead to a dramatic narrowing of spectral lines, giving rise to a potential new contrast mechanism for the rapidly emerging new field of mid-infrared microspectroscopy using QCLs.

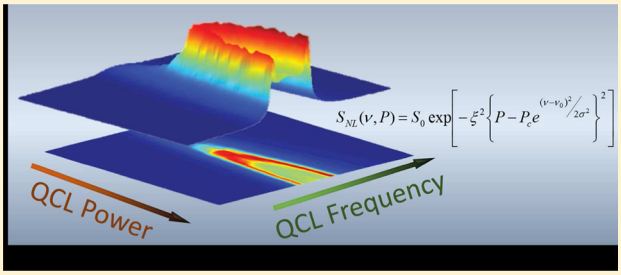

KEYWORDS: *photothermal spectroscopy, infrared spectroscopy, quantum cascade lasers, Zharov splitting, pitchfork bifurcation, nonlinear spectroscopy, liquid crystal*

Photothermal spectroscopy[1] has rapidly emerged as the most sensitive label-free optical spectroscopic method rivaling fluorescence spectroscopy particularly for nonradiative excited states. A nonequilibrium state is created in a sample by the absorption of a modulated pump laser and detected using the scatter[2] of a probe laser. When the pump laser is pulsed periodically, phase-lock methods allow the resultant nonequilibrium steady state to be studied with high sensitivity. In linear photothermal spectroscopy, the scattered probe signal is a linear function of the pump power with reported sensitivity down to the single molecule level at room temperature.[3,4] Recognition of the advantages of sensitivity and label-free nature have led to rapid development of linear photothermal methods in the visible region, both for spectroscopy and microscopy.[5−8] Photothermal spectroscopy has been used to characterize weak absorption[9−11] in solids and liquids and for spectroscopy of heme proteins and imaging in mitochondria.[5,6] Zharov[12−15] and co-workers have extended photothermal and photoacoustic spectroscopy to the nonlinear regime with reported splitting and sharpening of photothermal spectral signatures in the visible. Nonlinear spectral methods have the potential to significantly enhance the range of applications of photothermal microscopy[16] and super resolution imaging.[17] We extend nonlinear photothermal methods into the mid-infrared region of the spectrum using a Quantum Cascade Laser (QCL) as the pump laser, and present a detailed study of the striking peak splitting phenomenon, called Zharov splitting, characterized by a sharpening of mid-infrared photothermal spectrum in a liquid crystal. The tunability and power control of the QCL allow us to study the peak splitting in greater detail than was possible before. We show that the peak splitting is analogous to a supercritical bifurcation in nonlinear dynamical systems, with a "mean field" exponent of 0.5. The observations raise the possibility of universal behavior in the nonequilibrium steady state.

Midinfrared photothermal spectroscopy is attractive because of characteristic vibrational molecular normal modes, especially in the so-called "fingerprint" region.[18] With the invention of tunable QCLs,[19,20] mid-infrared spectroscopy is poised for rapid growth. The spectral brightness of these table-top QCL sources exceeds that of synchrotrons and other large relativistic electron-accelerator-based sources.[21] Indium antimonide (InSb) or mercury−cadmium−telluride (MCT)[18] liquid-nitrogen cooled detectors are intrinsically less sensitive than the best available photodetectors in the visible. A further attraction of photothermal spectroscopy is that it facilitates the use of sensitive room-temperature optical detectors for infrared spectroscopy.

Received: April 10, 2014
Published: July 18, 2014

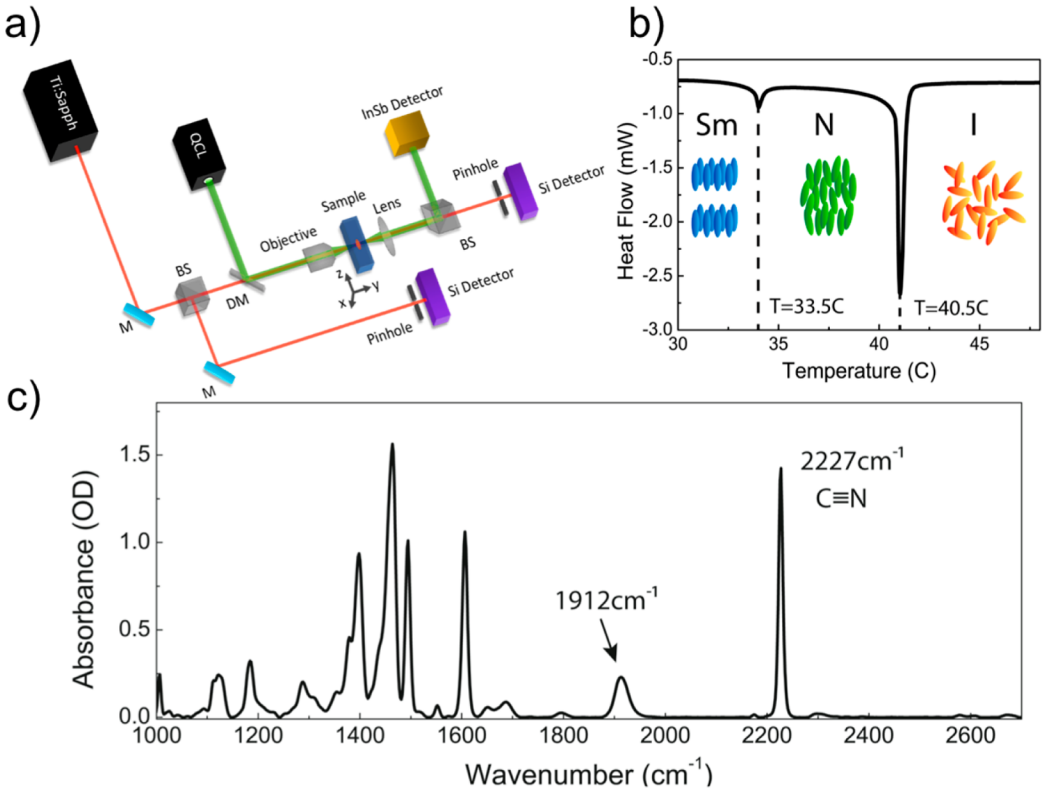

Figure 1. (a) Experimental setup for photothermal detection. The modulated QCL pump beam and Ti:sapphire probe beam are coaligned with the dichroic mirror and focused onto the sample by a special ZnSe objective. M-mirror, DM-dichroic mirror, and BS-beamsplitter. (b) Differential scanning calorimetry of 8CB liquid crystal showing three phases with an illustration of the orientations of the molecule director in the smectic-A phase (SmA), the nematic phase (N), and the isotropic phase (I). (c) FTIR absorption spectrum of 8CB.

Recently, we have reported on QCL-based photothermal heterodyne mid-infrared spectroscopy.[22]

MATERIALS AND METHODS

The experimental setup for both nonlinear and linear photothermal IR spectroscopy is shown in Figure 1a. A tunable Quantum Cascade Laser source tuned to a selected intrinsic absorption band serves as the modulated pump beam. The QCL was operated in pulse mode, with 500 ns pulses with a repetition rate of up to 100 kHz, corresponding to a maximum duty cycle of 5%. Absorption in the sample causes a thermally induced nonequilibrium change Δn in the refractive index experienced by a collinear probe beam, tuned to a wavelength far from any resonance. The nonequilibrium change arises from both a change in temperature within a particular phase of the liquid crystal or from a change in the phase of the liquid crystal, as explained below. The probe beam, provided by a Ti:sapphire laser tuned to 800 nm in cw mode, experiences scattering due to Δn, which can be detected by measuring the modulated scattered probe intensity, either in homodyne detection with the resultant signal being proportional to Δn^2 or in heterodyne detection[2] where the signal is proportional to Δn.

Cyanobiphenyls form a well-studied class of thermotropic liquid crystals, with rich phase behavior,[23−25] which we have used in our photothermal[22] and plasmonics studies.[26,27] The liquid crystal 4-octyl-4′-cyanobiphenyl (8CB) undergoes well-known phase transitions, from smectic-A phase (SmA) to nematic phase (N) at 306.5 K and then to the isotropic phase (I) at 313.5 K[25,28,29] shown by the endotherms in differential scanning calorimetry (DSC) measurements in Figure 1b. For mid-IR photothermal studies, the 4-octyl-4′-cyanobiphenyl (8CB) liquid crystal sample was sandwiched between cleaned CaF_2 windows with 50 μm Mylar spacer. In the absence of rubbing or surface coating, the molecular alignment of the bulk is homogeneous, with no preferred direction at either of the two CaF_2 windows. Observation with visible light under crossed polarizers did not show homeotropic alignment of the sample as a whole (see Supporting Information, SI). The FTIR absorbance spectrum in Figure 1c shows a weak combination band, thought to arise from out-of-plane CH vibrations[30] centered at 1912 cm^{-1} (also Figure S1) and lies within the tuning range of the QCL laser with a molar extinction coefficient of 14.9 M^{-1} cm^{-1}. The base temperature of the sample is controlled using a circulating water bath. The photothermal signal due to the weak mid-infrared combination mode (Figure 1c) could be observed in all of the phases of 8CB. Previous photothermal studies of liquid crystals required the use of a dye[31] or gold nanoparticles[32] and a detailed understanding of guest−host interactions.[33] In contrast, photothermal infrared spectroscopy[22,34] is inherently label-free.

RESULTS

Figure 2 shows a sequence of 25 photothermal absorption spectra of 8CB at a temperature of 29 °C in the smectic-A phase as the current in the QCL and, hence, the incident IR power is increased. The intensity at the sample varied over a range 0.1−1.2 × 10^4 W/cm^2. The observed photothermal signal depends on the power absorbed by the sample at each frequency. For a given value of the QCL current, the incident power at each frequency was independently measured using the cryogenically cooled

dx.doi.org/10.1021/ph500114h | ACS Photonics 2014, 1, 696−702

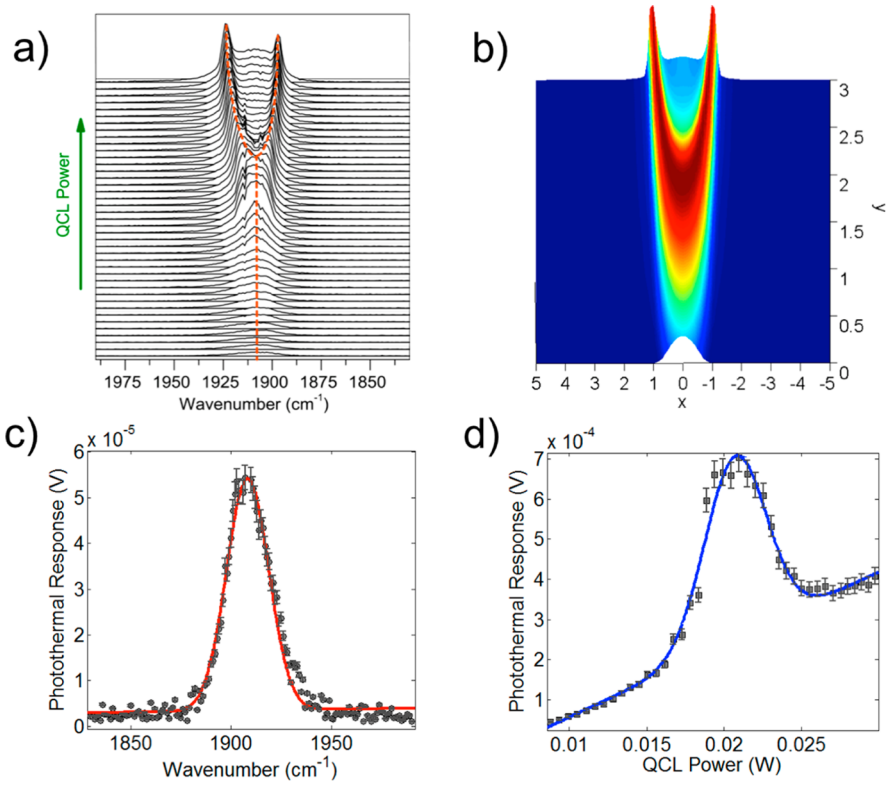

Figure 2. (a) Linear and nonlinear regimes in Photothermal IR spectroscopy in 8CB at 29 °C. Spectra have been displaced vertically for clarity. At small QCL current, the photothermal spectrum closely follows the linear FTIR spectrum. At high currents, the spectrum indicates a bifurcation. The critical power at the peak frequency is at incident QCL power of 0.021 W. (b) Surface plot of the calculated photothermal signal S_{Tot} using the phenomenological model described in the paper. The scaled dimensionless QCL frequency x and the scaled dimensionless QCL power y are defined in the text. (c) Photothermal response at a low incident pump power of 0.01 W, where the response is still in the linear regime. Solid line is a fit to a Gaussian function in frequency with a fwhm 37 ± 2 cm^{-1}. (d) Photothermal response above the bifurcation transition for 29 °C, as a function of incident infrared power P, for a fixed frequency at the peak of the IR absorption band 1912 cm^{-1}. The solid line is a fit to a term linear in the power to represent the linear response and a Gaussian form for the nonlinear component, as described in the text.

detector and calibrated using a power meter in the absence of the sample cell.

The protocol for acquiring the data is described in Supporting Information. At low pump power, the photothermal spectrum is identical to the linear IR absorption spectrum (Figure S2a). The linear spectrum was measured in two different ways—using a commercial FTIR spectrometer and by measuring the transmitted IR signal from the QCL using an InSb cryogenically cooled detector in single beam mode. The IR signal was measured simultaneously along with the photothermal response. The calculation from a phenomenological mean-field model for the nonlinear photothermal response is also shown in Figure 2b. Figure 3 shows the transition in the photothermal response between the linear and nonlinear regime in greater detail.

Four different regimes can be identified: (i) As the QCL current is increased, the magnitude of the PTS signal at the peak absorption frequency 1912 cm^{-1} increases linearly at first, but the band shape is unchanged. (ii) At higher currents, it can be seen that the amplitude of the PTS also has a weak quadratic dependence (Figure 3a), but the shape of the spectral band is still unaltered. (iii) Above a first threshold evident in Figure 3, a narrow spike appears centered near the absorption peak frequency. (iv) As the absorbed power is increased beyond a critical threshold of absorbed power P_c, the narrow peak splits into two branches and each branch sharpens still further. Figure 3b shows a superposition of the photothermal spectrum in the linear and nonlinear regimes. The spectra are normalized to illustrate the dramatic narrowing of the split red and blue-shifted peaks in the nonlinear spectrum, compared to the linear absorption spectrum. The separation $\Delta\nu$ between the peak center frequencies of each of the two branches increases with power P. We find that $\Delta\nu \propto (P - P_c)^{1/2}$ (Figure 3c,d). For a given base sample temperature T, the critical threshold absorbed power P_c required for peak splitting is remarkably reproducible and is a function of T.

In order to investigate the nature of the bifurcation, we measured the photothermal response as a function of temperature, QCL frequency and absorbed power. Figure 4 shows the peak splitting response for a selected set of sample base temperatures (Figure S3). At each temperature, the peaks split and display the same $\Delta\nu \propto (P - P_c)^{1/2}$ dependence on the incident QCL laser power P. The robustness of the scaling exponent was tested by fitting to a generalized power law of the form $\Delta\nu = b(P - P_c)^{\beta}$ where the exponent β is allowed to vary and is not constrained (Figure 4a–e), along with the parameter b. A histogram of the exponents under different experimental conditions gave a range for $\beta = 0.5 \pm 0.01$, independent of temperature (Figure 4d). The critical power decreased linearly as the sample temperature is raised from 28 to 32 °C, approaching the SmA-N phase transition temperature (Figure 4e). Above about 31 °C, peak splitting occurs in the photothermal spectrum even just above the lasing threshold of the QCL. To summarize, all the peak splitting data can be fitted with a single universal

dx.doi.org/10.1021/ph500114h | ACS Photonics 2014, 1, 696–702

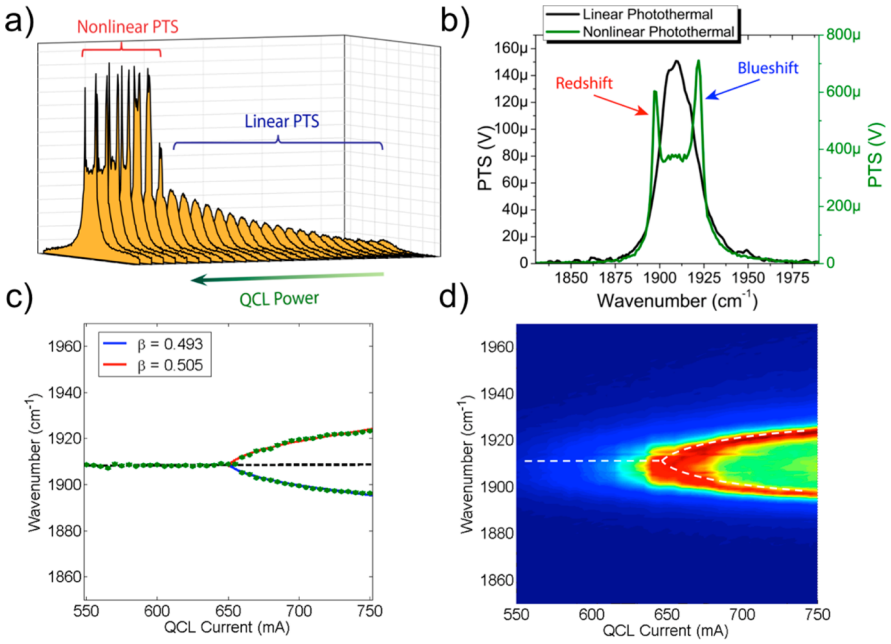

Figure 3. (a) 3-D plot of the photothermal signal as a function of the QCL frequency ν in wavenumbers, and as a function of QCL power P in 8CB at 29 °C. The linear and nonlinear regimes are described in the text. (b) Superposed linear and nonlinear photothermal spectra showing Zharov splitting and ultrasharp narrowing in both the red and blue-shifted nonlinear photothermal split peaks. (c) Peak frequency as a function of QCL current. The dashed line is a fit of the peak frequency in the linear regime. The error bars on the frequency are ±1 cm^{-1}. Solid lines are fits to a phenomenological model in which the separation between the bifurcated peaks $\Delta\nu$ is proportional to $(P-P_c)^{\beta}$ for $P > P_c$. The fitted value of the exponent β is 0.5 ± 0.01 (see Figure 4). (d) Observed data showing the peak splitting phenomenon projected onto the $\nu-I$ plane, where I is the QCL current. Increasing QCL current results in increasing incident power P, with the calibration between P and I for each QCL frequency shown in Supporting Information (Figure S4).

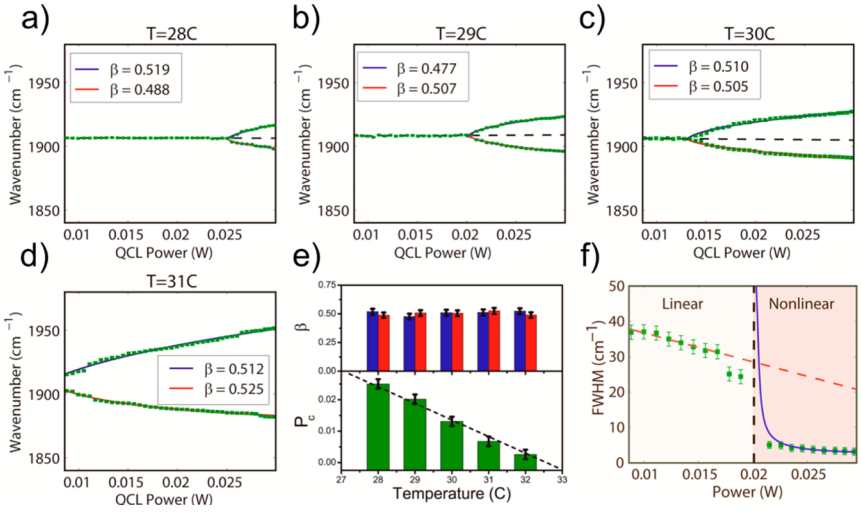

Figure 4. (a–d) Analysis of nonlinear photothermal bifurcation at different sample temperatures 28–31 °C. Data points are obtained, as in Figure 3, and the fits are solid lines; $\Delta\nu$ is proportional to $(P - P_c)^{\beta}$, where the exponent β was allowed to vary. (e) Histogram of the experimentally derived exponents at different temperatures for both the blue-shifted(blue bars) and red-shifted (red bars) branches of the bifurcation. The exponent $\beta = 0.5 \pm 0.01$. Also shown is a histogram of the fitted values of P_c at different temperatures. (f) Full-width-at-half-maximum (fwhm) of the linear PTS spectrum, and the blue-shifted nonlinear branch following bifurcation, at 29 °C. The solid line is a fit to the phenomenological model with the fwhm is proportional to $(P - P_c)^{-1/2}$.

curve in which the peak frequency split can be fit to form $\Delta\nu = b(P - P_c)^{\beta}$, with an apparently universal temperature independent exponent, $\beta = 0.5$.

DISCUSSION

While it is initially tempting to conclude that our observations listed above are specific to phase transitions in liquid crystals, the observation of the peak splitting phenomenon by Zharov and co-workers on a completely different aqueous physical system suggests that the phenomenon is rather general, requiring only the nucleation of a higher temperature phase. The exponent associated with the peak splitting phenomenon is observed in our work for a nonequilibrium system, complementary to equilibrium studies in the rich literature on effective critical exponents

dx.doi.org/10.1021/ph500114h | ACS Photonics 2014, 1, 696–702

belonging to the 3-D XY universality class near the smectic A-nematic phase transition in bulk 8CB,[25] and in other systems.[35] The observed exponent of 0.5 is generally expected for dynamical systems that exhibit pitchfork bifurcation,[36] which is intimately related to the mean field dynamics theory[37] of an equilibrium order parameter with Z_2 symmetry, such as the Ising model near a phase transition. The framework for analysis of our nonequilibrium steady state experiments is set by the prior work on nanoparticles in aqueous media in the visible region of the electromagnetic spectrum,[12] where the peak splitting effect was attributed to reduced forward scattering due to the formation of "nanobubbles" caused by laser heating. The formation of bubbles, with a discontinuous boundary in the refractive index between two phases, results in significant elastic backscatter of the probe beam due to a combination of Mie scattering and multiple scattering events. The contribution to forward elastic scatter of the probe beam then decreases, and the observed PTS signal also decreases. Optical elastic scattering into large magnitude **q**-vectors from thermally generated clusters[12] thus reduces the photothermal response in the nonlinear regime. Forward elastic scattering can also be reduced because of enhanced director fluctuations in the nematic phase, as pointed out by an anonymous reviewer. A simple way to think about this rather complex explanation is the following: the PTS signal is due to the formation of a thermal lens;[1] creation of bubbles destroys the thermal lens leading to a loss in the signal.[12] Such a mechanism for peak splitting is expected to hold for mid-infrared photothermal spectroscopy as well. Based on this analysis, we expect that the first observable reduction in the scattered photothermal signal to coincide with the peak of the infrared pump absorption, that is, at 1912 cm^{-1}, as shown in Figure 3b. The microscopic mechanism for bubble or cluster generation, and the scattering cross-section, varies from sample to sample. The observed peak splitting phenomenon shares some general aspects of spectral hole burning,[38] but the approach here is qualitatively different. In conventional hole-burning spectroscopy, the density of states of the chromophore is altered by an external laser that "burns a hole" in the absorption or emission spectrum. In our experiments, as noted above, the transmitted mid-infrared radiation detected by a cryogenically cooled detector, does not show any sign of the peak splitting phenonmenon. Only the forward scattered probe shows this effect. Thus, the density of states of the chromophore is not altered, in contrast to conventional hole-burning spectroscopy.

In classical hole burning the imaginary part of the dielectric function at the probe frequency is altered (i.e., reduced absorption). In our case the real part of the dielectric response at the probe frequency, related to the refractive index, is altered. In support of this hypothesis, we note below that the spectrum measured by the cryogenic infrared detector does *not* show peak splitting (Figure S5); only the scattered photothermal response does.

To understand why peak splitting occurs in the photothermal spectrum, but not in the IR absorption spectrum that is being simultaneously monitored, the discussion in the above paragraph suggests a simple model. The nonlinear contribution S_{NL} to the observed photothermal scattering signal in Figure 3a can be considered to be a function of two variables $S_{NL}(\nu, P)$, where ν is the infrared QCL frequency and P is the incident power of the QCL that serves as control parameter. The dependence on other experimental variables like the temperature, probe wavelength and probe power is implicit in the parametrization of the model. At a fixed QCL frequency close to the peak of the infrared band, the observed nonlinear contribution can be fit to a phenomenological Gaussian functional form, as shown in Figure 2c.

$$S_{NL}(\nu, P) = S_0 e^{-\xi^2[P - P_T(\nu)]^2} \tag{1}$$

For a fixed QCL frequency, the parameter ξ sets the width of the Gaussian as a function of incident QCL power. S_0 is the amplitude of the observed signal. The parameter P_T depends on the IR QCL frequency and has a simple interpretation: it represents the incident QCL power at which the maximum photothermal signal is detected. Physically it represents a threshold power above which scatter from nanobubble formation leads to a decrease in the forward scattered probe signal. Since the bubble formation depends on the power absorbed in the sample, we expect P_T to be the smallest when the QCL is tuned to the peak of the resonance frequency ~1912 cm^{-1}. As the QCL frequency is detuned from resonance, increasingly greater incident power is needed to reach the same threshold for bubble formation. It is then obvious that the functional dependence of P_T on the frequency is the reciprocal of the linear FTIR absorbance spectrum. For the specific case of the combination band studied here, the linear IR spectrum is approximately a Gaussian centered at the peak IR frequency $\sim e^{-(\nu-\nu_0)^2/2\sigma^2}$, where σ is determined by the full-width-at-half-maximum (fwhm) of the linear FTIR spectrum. The threshold parameter in eq 1 is then given by $P_T(\nu) = P_c e^{+(\nu-\nu_0)^2/2\sigma^2}$ leading to a simple analytic functional form for the nonlinear photothermal signal:

$$S_{NL}(\nu, P) = S_0 \exp\left[-\xi^2\left\{P - P_c e^{(\nu-\nu_0)^2/2\sigma^2}\right\}^2\right] \tag{2}$$

In the simplest analysis, the total experimentally observed signal S_{Tot} is a sum of the nonlinear component S_{NL}, and the linear response S_L, $S_{Tot} = S_L + S_{NL}$. In this analysis the linear response is of the form $S_L(\nu, P) = f_\lambda P e^{-(\nu-\nu_0)^2/2\sigma^2}$, where the factor f_λ depends on the probe wavelength, probe power, collection, and geometric factors, as discussed extensively by Berciaud et al.[2] In simply summing the linear and nonlinear responses, interference effects are neglected. Figure 3d shows a surface plot of the sum of the linear and nonlinear contributions $S_{Tot} = S_L + S_{NL}$. As seen in Figure 3d, the function captures the essence of the peak splitting phenomenon and yields the correct value of the critical exponent 0.5. S_0 is independent of the QCL frequency. The peak frequency of the nonlinear photothermal spectrum S_{NL} can be obtained easily from the analytic form. To make contact with well-established formalism of nonlinear maps and dynamical systems, we consider the formal problem of finding the maximum of function. Defining a "free energy" $F = -\ln S_{NL}(\nu, P)$, the maxima are then the minima of F at constant power P, given by $[\partial F/\partial \nu]|_P = 0$. The roots of the resulting algebraic equation give the peak frequency. Peak splitting occurs when the equation has multiple roots. Considering the functional form as a nonlinear dynamical map, expressed in terms of dimensionless variables x,y

$$\begin{aligned} &x = (\nu - \nu_0)^2/2\sigma^2, \\ &y = P/P_c \Rightarrow S = S_0 \exp[-\zeta^2(y - e^{x^2})^2] \Rightarrow \\ &F = \zeta^2(y - e^{x^2})^2 \end{aligned} \tag{3}$$

dx.doi.org/10.1021/ph500114h | ACS Photonics 2014, 1, 696−702

Close to the maximum $x = 0$, the map is clearly quadratic

$$F = \zeta^2(y - 1 - x^2 + \cdots)^2 \Rightarrow$$
$$F/\zeta^2 \approx (y-1)^2 - 2(y-1)x^2 + x^4$$
$$\left.\frac{\partial F}{\partial x}\right|_y = 0 \quad \Rightarrow -4(y-1)x + 4x^3 = 0$$
$$\Rightarrow \begin{cases} x = 0 \\ x_\pm = \pm\sqrt{y-1} \end{cases} \tag{4}$$

Expressed in terms of the observed variables P and QCL frequency ν, it can be seen that (i) when P is less than P_c the peak frequency is at ν_0, which is the maximum of the linear FTIR spectrum; (ii) when P exceeds P_c, the peak frequency of the nonlinear scattering signal is split into two branches, with $\Delta\nu = b(P - P_c)^\beta$ as observed. The exponent 0.5 arises mainly from the symmetry. The Gaussian nature of the functional forms are not important, so long as they belong to the universality class of quadratic maps. The threshold power P_c required to create a bubble of the higher temperature phase depends on how far the sample temperature is from the SmA-N phase transition temperature. The parameter P_c, which is determined in the nonequilibrium steady state, is linked closely to an underlying equilibrium phase transition. Remarkably, this simple model also reproduces the observed sharpening of the nonlinear response observed in Figure 4f. The formation of the nanobubble is significant not only for the sharpening observed in the nonlinear photothermal effect, but also in the related nonlinear photoacoustic resonances observed in ref 12.

Limitations. The "mean field" approach correctly predicts the sharpening of the observed nonlinear photothermal spectral peaks above the bifurcation. Figure 3 shows that the widths of the nonlinear peaks, estimated by the full-width-at-half-maximum (fwhm), decrease as the incident QCL power increases. A straightforward calculation of the fwhm using the model of eq 2 confirms this. Quantitatively, just above the bifurcation transition, each of the two bifurcated peaks has a line width that diverges as $\Delta x_\pm = \langle (x - x_\pm)^2 \rangle^{1/2} \propto (y-1)^{-\beta'}$, where the exponent β' is also 0.5. Recasting this in terms of the experimental unscaled variables, the width of the narrow peaks decreases with increasing QCL power P as $(P - P_c)^{-1/2}$. The width of the ultrasharp features in our experiments is determined primarily by the ~1 cm^{-1} line width and repeatability of the QCL laser frequency and the precision with which the QCL power can be controlled. Studies of line widths suggest the limitations of the approach. While Figure 3b confirms the sharpening experimentally, there is an observed asymmetry in the line widths in the upper and lower branches of the bifurcation, in studies performed at fixed QCL current. In the data shown in Figure 3, the red-shifted peak has a line width of 1.7 cm^{-1}, compared to the 2.5 cm^{-1} line width of the blue-shifted peak. The asymmetry is due to several reasons. The first is a systematic experimental effect because, even at constant QCL current, the IR power incident at the two peak frequencies $\nu_\pm$ are slightly different (Figure S4). Also, due to a small offset between the maximum of the frequency in the Gain curve of the QCL and the 1912 cm^{-1} IR absorption band peak. Correction for this systematic experimental effect does not however completely remove the observed asymmetry. A second contribution is due to an underlying weak asymmetry in the IR absorption spectrum (Figure S1b), which is not taken into account in eq 2. Extension to nonsymmetric vibrational spectra may be done by expressing the threshold power in terms of the appropriate spectral moments and will lead to corrections for the exponent. The analysis here must therefore be regarded as a first step, with extensions necessitated by further observations on other nonlinear photothermal systems, accounting for fluctuations and finite size effects in systems driven into nonequilibrium steady state. The bifurcation and dramatic sharpening of infrared absorption spectroscopy may be universal with applications to biological systems and materials science and engineering.

■ ASSOCIATED CONTENT

Supporting Information

Further details of the data acquisition, data analysis, and theoretical model. This material is available free of charge via the Internet at http://pubs.acs.org.

■ AUTHOR INFORMATION

Corresponding Author

*E-mail: shyam@bu.edu.

Notes

The authors declare no competing financial interest.

■ ACKNOWLEDGMENTS

We acknowledge support from NIH Grant No. 1 R21 EB013381-01 and NSF I/UCRC Grant No. NSF IIP-1068070. We thank T. Jeys and V. Liberman, MIT Lincoln Laboratories, for discussions and the generous loan of the QCL system.

■ REFERENCES

(1) Bialkowski, S. E. *Photothermal Spectroscopy Methods for Chemical Analysis*; Wiley: New York, 1996.

(2) Berciaud, S.; Lasne, D.; Blab, G. A.; Cognet, L.; Lounis, B. Photothermal Heterodyne Imaging of Individual Metallic Nanoparticles: Theory versus Experiment. *Phys. Rev. B* **2006**, *73*, 45424.

(3) Armani, A. M.; Kulkarni, R. P.; Fraser, S. E.; Flagan, R. C.; Vahala, K. J. Label-Free, Single-Molecule Detection with Optical Microcavities. *Science* **2007**, *317*, 783−787.

(4) Gaiduk, A.; Yorulmaz, M.; Ruijgrok, P. V.; Orrit, M. Room-Temperature Detection of a Single Molecule's Absorption by Photothermal Contrast. *Science* **2010**, *330*, 353−356.

(5) Lasne, D.; Blab, G. A.; De Giorgi, F.; Ichas, F.; Lounis, B.; Cognet, L. Label-Free Optical Imaging of Mitochondria in Live Cells. *Opt. Express* **2007**, *15*, 14184−14193.

(6) Lu, S.; Min, W.; Chong, S.; Holtom, G. R.; Xie, X. S. Label-Free Imaging of Heme Proteins with Two-Photon Excited Photothermal Lens Microscopy. *Appl. Phys. Lett.* **2010**, *96*, 113701.

(7) Cognet, L.; Tardin, C.; Boyer, D.; Choquet, D.; Tamarat, P.; Lounis, B. Single Metallic Nanoparticle Imaging for Protein Detection in Cells. *Proc. Natl. Acad. Sci. U.S.A.* **2003**, *100*, 11350−11355.

(8) Boyer, D.; Tamarat, P.; Maali, A.; Lounis, B.; Orrit, M. Photothermal Imaging of Nanometer-Sized Metal Particles Among Scatterers. *Science* **2002**, *297*, 1160−1163.

(9) Cabrera, H.; Cordido, F.; Velásquez, A.; Moreno, P.; Sira, E.; López-Rivera, S. A. Measurement of the Soret Coefficients in Organic/water Mixtures by Thermal Lens Spectrometry. *C. R. Mec.* **2013**, *341*, 372−377.

(10) Berciaud, S.; Cognet, L.; Poulin, P.; Weisman, R. B.; Lounis, B. Absorption Spectroscopy of Individual Single-Walled Carbon Nanotubes. *Nano Lett.* **2007**, *7*, 1203−1207.

(11) Jackson, W. B.; Amer, N. M.; Boccara, a C.; Fournier, D. Photothermal Deflection Spectroscopy and Detection. *Appl. Opt.* **1981**, *20*, 1333−1344.

(12) Zharov, V. P. Ultrasharp Nonlinear Photothermal and Photoacoustic Resonances and Holes beyond the Spectral Limit. *Nat. Photonics* **2011**, *5*, 110−116.

(13) Nedosekin, D. A.; Galanzha, E. I.; Ayyadevara, S.; Shmookler Reis, R. J.; Zharov, V. P. Photothermal Confocal Spectromicroscopy of Multiple Cellular Chromophores and Fluorophores. *Biophys. J.* **2012**, *102*, 672−681.
(14) Shao, J.; Griffin, R. J.; Galanzha, E. I.; Kim, J.-W.; Koonce, N.; Webber, J.; Mustafa, T.; Biris, A. S.; Nedosekin, D. A.; Zharov, V. P. Photothermal Nanodrugs: Potential of TNF-Gold Nanospheres for Cancer Theranostics. *Sci. Rep.* **2013**, *3*, 1293.
(15) Hleb, E. Y.; Hu, Y.; Drezek, R. A.; Hafner, J. H.; Lapotko, D. O. Photothermal Bubbles as Optical Scattering Probes for Imaging Living Cells. *Nanomedicine (London)* **2008**, *3*, 797−812.
(16) Rajakarunanayake, Y. N.; Wickramasinghe, H. K. Nonlinear Photothermal Imaging. *Appl. Phys. Lett.* **1986**, *48*, 218.
(17) Nedosekin, D. A.; Galanzha, E. I.; Dervishi, E.; Biris, A. S.; Zharov, V. P. Super-Resolution Nonlinear Photothermal Microscopy. *Small* **2014**, DOI: 10.1002/smll.201300024.
(18) Griffiths, P. R.; de Haseth, J. A. *Fourier Transform Infrared Spectrometry*, 2nd ed.; Wiley: New York, 2007.
(19) Faist, J.; Capasso, F.; Sivco, D. L.; Sirtori, C.; Hutchinson, A. L.; Cho, A. Y. Quantum Cascade Laser. *Science* **1994**, *264*, 553.
(20) Capasso, F.; Gmachl, C.; Paiella, R.; Tredicucci, A.; Hutchinson, A. L.; Sivco, D. L.; Baillargeon, J. N.; Cho, A. Y.; Liu, H. C. New Frontiers in Quantum Cascade Lasers and Applications. *IEEE J. Sel. Top. Quantum Electron.* **2000**, *6*, 931−947.
(21) Carr, G. L.; Dumas, P.; Hirschmug, C. J.; Williams, G. P. Infrared Synchrotron Radiation Programs at the National Synchrotron Light Source. *Nuovo Cimento D* **1998**, *20*, 375−395.
(22) Mertiri, A.; Jeys, T.; Liberman, V.; Hong, M. K.; Mertz, J.; Altug, H.; Erramilli, S. Mid-Infrared Photothermal Heterodyne Spectroscopy in a Liquid Crystal Using a Quantum Cascade Laser. *Appl. Phys. Lett.* **2012**, *101*, 44101.
(23) Babkov, L. M.; Gnatyuk, I. I.; Trukhachev, S. V. Investigation of 4′-*N*-Alkyl-4-cyanobiphenyls Structure Features by IR Spectroscopy Methods. *J. Mol. Struct.* **2005**, *744*−*747*, 425−432.
(24) Thomas, M.; Richardson, H. H. Two-Dimensional FT-IR Correlation Analysis of the Phase Transitions in a Liquid Crystal, 4′-*N*-Octyl-4-cyanobiphenyl (8CB). *Vib. Spectrosc.* **2000**, *24*, 137−146.
(25) Kutnjak, Z.; Kralj, S.; Lahajnar, G.; Zumer, S. Thermal Study of Octylcyanobiphenyl Liquid Crystal Confined to Controlled-Pore Glass. *Fluid Phase Equilib.* **2004**, *222*−*223*, 275−281.
(26) Cetin, A. E.; Mertiri, A.; Huang, M.; Erramilli, S.; Altug, H. Thermal Tuning of Surface Plasmon Polaritons Using Liquid Crystals. *Adv. Opt. Mater.* **2013**, *1*, 915−920.
(27) Çetin, A. E.; Yanik, A. A.; Mertiri, A.; Erramilli, S.; Müstecaplıoğlu, O. E.; Altug, H. Field-Effect Active Plasmonics for Ultracompact Electro-Optic Switching. *Appl. Phys. Lett.* **2012**, *101*, 121113.
(28) Davidov, D.; Safinya, C. R.; Kaplan, M.; Dana, S. S.; Schaetzing, R.; Birgeneau, R. J.; Litster, J. D. High-Resolution X-ray and Light-Scattering Study of Critical Behavior Associated with the Nematic−Smectic-A Transition in 4-Cyano-4′-octylbiphenyl. *Phys. Rev. B* **1979**, *19*, 1657.
(29) Thoen, J.; Marynissen, H.; Van Dael, W. Temperature Dependence of the Enthalpy and the Heat Capacity of the Liquid-Crystal Octylcyanobiphenyl (8CB). *Phys. Rev. A* **1982**, *26*, 2886.
(30) Frunza, L.; Kosslick, H.; Bentrup, U.; Pitsch, I.; Fricke, R.; Frunza, S.; Schönhals, A. Surface Layer in Composites Containing 4-*N*-Octyl-4′-cyanobiphenyl. FTIR Spectroscopic Characterization. *J. Mol. Struct.* **2003**, *651*−*653*, 341−347.
(31) Yelleswarapu, C. S.; Kothapalli, S.-R.; Aranda, F. J.; Rao, D. V. G. L. N.; Vaillancourt, Y. R.; Kimball, B. R. Phase Contrast Imaging Using Photothermally Induced Phase Transitions in Liquid Crystals. *Appl. Phys. Lett.* **2006**, *89*, 211116.
(32) Parra-Vasquez, A. N. G.; Oudjedi, L.; Cognet, L.; Lounis, B. Nanoscale Thermotropic Phase Transitions Enhancing Photothermal Microscopy Signals. *J. Phys. Chem. Lett.* **2012**, *3*, 1400−1403.
(33) Truong, T.; Xu, L.; Shen, Y. Early Dynamics of Guest−Host Interaction in Dye-Doped Liquid Crystalline Materials. *Phys. Rev. Lett.* **2003**, *90*, 193902−.
(34) Farahi, R. H.; Passian, A.; Tetard, L.; Thundat, T. Pump−Probe Photothermal Spectroscopy Using Quantum Cascade Lasers. *J. Phys. D: Appl. Phys.* **2012**, *45*, 125101.
(35) Kumar, S.; Kang, S. W. Structure: Liquid Crystals. *Encycl. Condens. Matter* **2005**, *3*, 111−120.
(36) Strogatz, S. H. Nonlinear Dynamics and Chaos: With Applications to Physics, Biology. *Chemistry, and Engineering*; Westview Press: Boulder, CO, 1994.
(37) Stanley, H. E. *Introduction to Phase Transitions and Critical Phenomena*; Oxford University Press: New York, 1987.
(38) Mukamel, S. *Principles of Nonlinear Optical Spectroscopy*; Oxford University Press: New York, 1999.